Supplementary Material

Co/Multi-walled carbon nanotubes/Polyethylene composites for microwave absorption: tuning the effectiveness of electromagnetic shielding by varying the components ratio

*Mariya A. Kazakova** [a, b], *Nina V. Semikolenova* [a], *Evgeniy Yu. Korovin* [c], *Viktor A. Zhuravlev* [c], *Alexander G. Selyutin* [a], *Dmitry A. Velikanov* [d], *Sergey I. Moseenkov* [a], *Andrey S. Andreev* [e], *Olga B. Lapina* [a], *Valentin I. Suslyaev* [c], *Mikhail A. Matsko* [a], *Vladimir A. Zakharov* [a], *Jean-Baptiste d'Espinose de Lacaillerie* [f]

[a] Boreskov Institute of Catalysis, SB RAS, Lavrentieva 5, Novosibirsk 630090, Russia

[b] Novosibirsk State University, Pirogova 2, Novosibirsk, 630090, Russia

[c] National Research Tomsk State University, Lenin Ave. 36, Tomsk, 634050, Russia

[d] Kirensky Institute of Physics, SB RAS, Akademgorodok St. 50, Krasnoyarsk, 660036, Russia

[e] TOTAL Research and Technology Feluy (TRTF), Zone Industrielle C, 7181 Feluy, Belgium

[f] Soft Matter Science and Engineering (SIMM), UMR CNRS 7615, ESPCI Paris, Université PSL, Sorbonne Université, 75005, Paris, France

* Corresponding author. Tel: +7383 326-97-50. E-mail: mas@catalysis.ru (Mariya A. Kazakova)

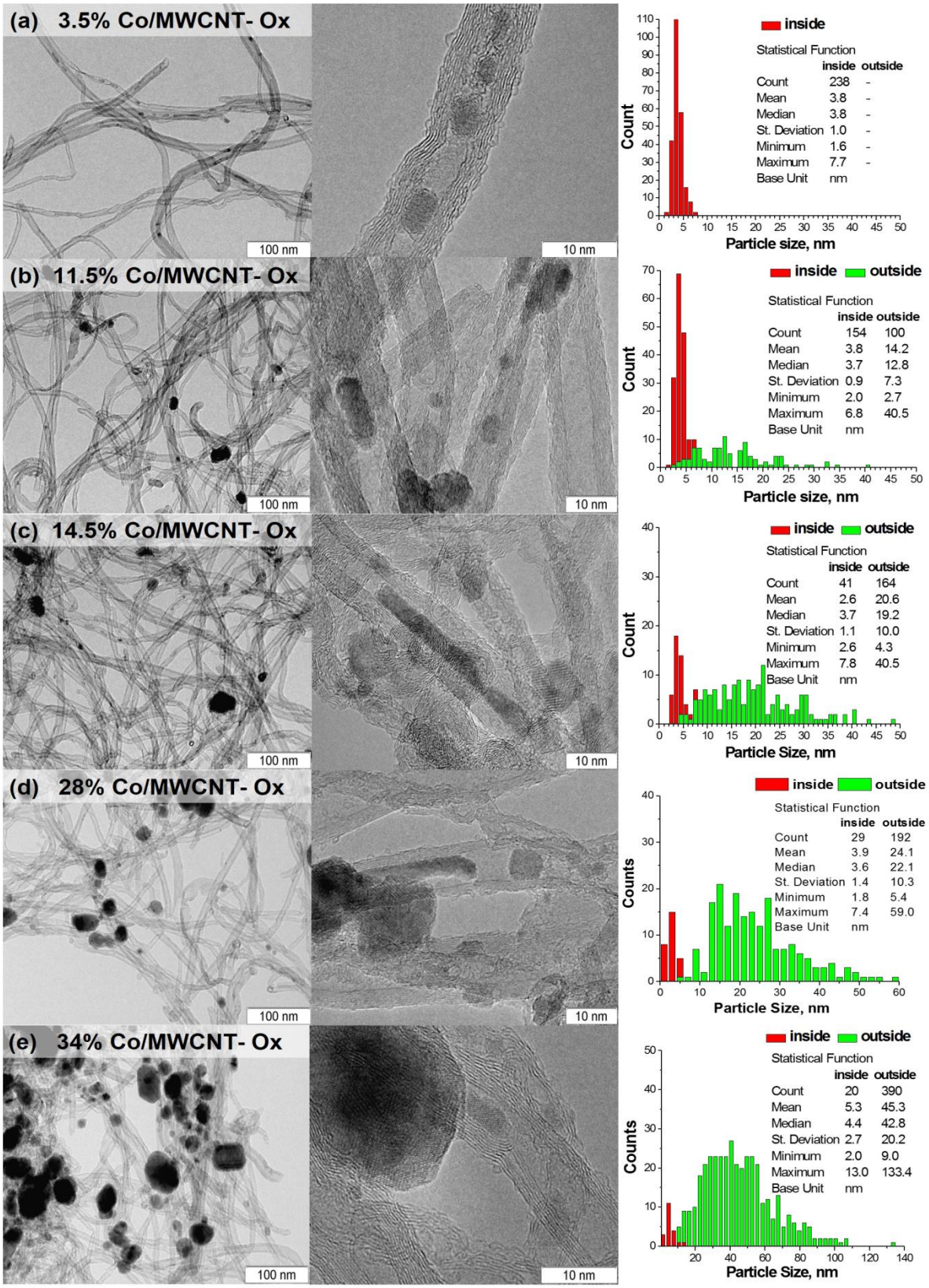

Fig. S1. TEM images and particle size distribution of Co nanoparticles embedded in MWCNT structure with different Co loading (3.5 - 34 wt.% according to XRF data).

In situ X-ray diffraction of Co reduction of the Co/MWCNT samples.

The crystal phase transformations of the cobalt phase during the reduction of impregnated MWCNT precursors were monitored *in situ* by XRD using a Bruker Advance D8 (Germany) equipped with the vertical theta geometry (Bragg-Brentano), Cu K-α radiation (λ=0.15418 nm). The samples were placed in an XRK 900 X-ray reaction chamber (Anton Paar, Austria). Heating was performed from room temperature to 700 °C at a rate of 12 °C/min under a flow of diluted H_2 (H_2 rate of 40 ml/sec). The scanned 2θ range was from 30° to 60° (in steps of 0.05° and a counting time of 3 s), thus permitting to capture the main reflections of Co metal (PDF 15-806), CoO (PDF 48-1719), Co_3O_4 (PDF 42-1467), and MWCNT (PDF 58-1638). Phase analysis was performed using the ICDD PDF-2 database. The X-ray patterns were interpreted using the Bruker Topas full profile analysis program. The contribution of the baseline was eliminated by conducting additional experiments on the original nanotubes. Additional interpretation of the data was carried out using the Fityk open source software.

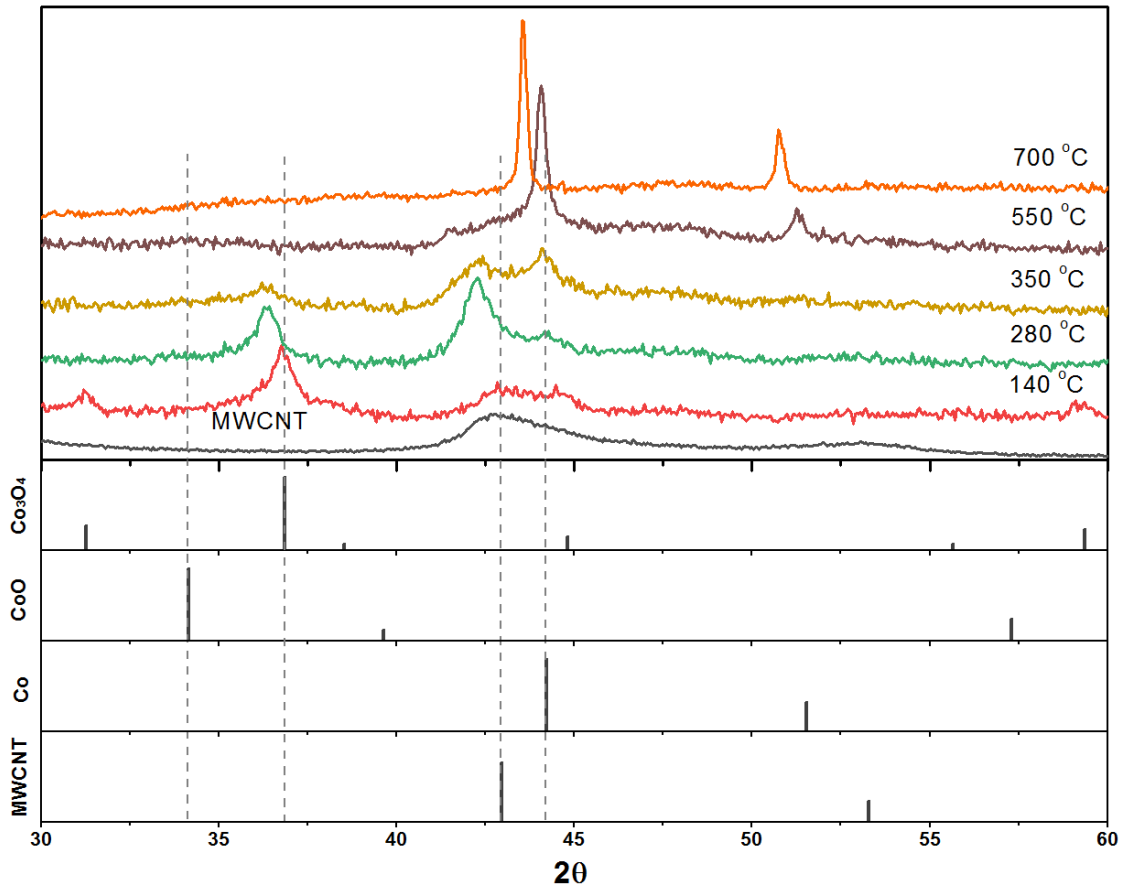

Fig. S2. *In situ* XRD pattern of the 14.5% Co/MWCNT sample during reduction in an hydrogen flow at various temperatures (140-700 °C).

Different fixation schemes of the Ti-containing polymerization catalyst on the surface of the MWCNT and Co/MWCNT samples

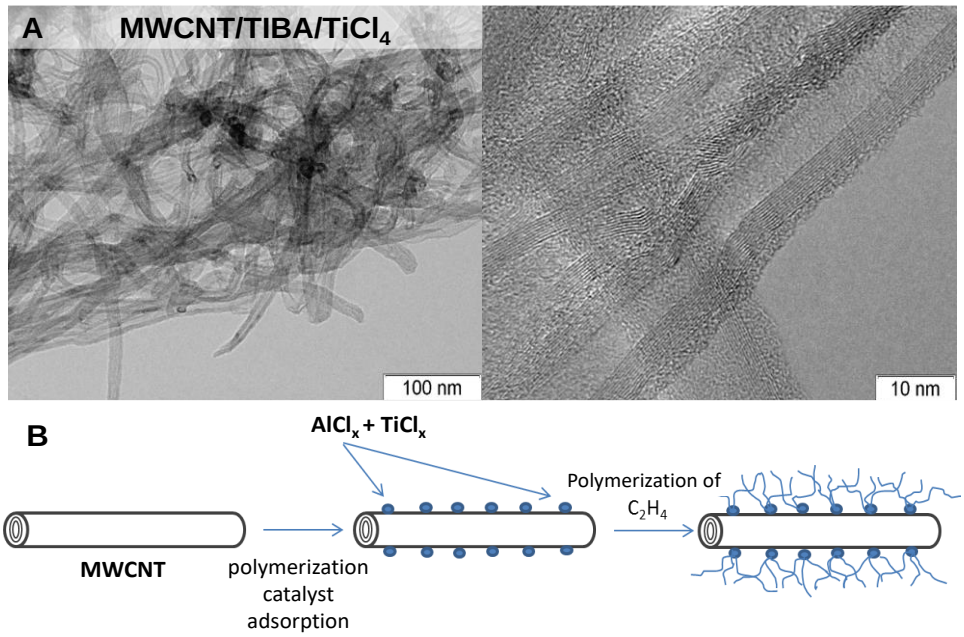

Fig. S3. A - TEM images of the polymerization catalytic system MWCNT/TIBA/$TiCl_4$; B – Schematic proposition of the localization of the Ti-containing polymerization catalyst on the surface of the MWCNT.

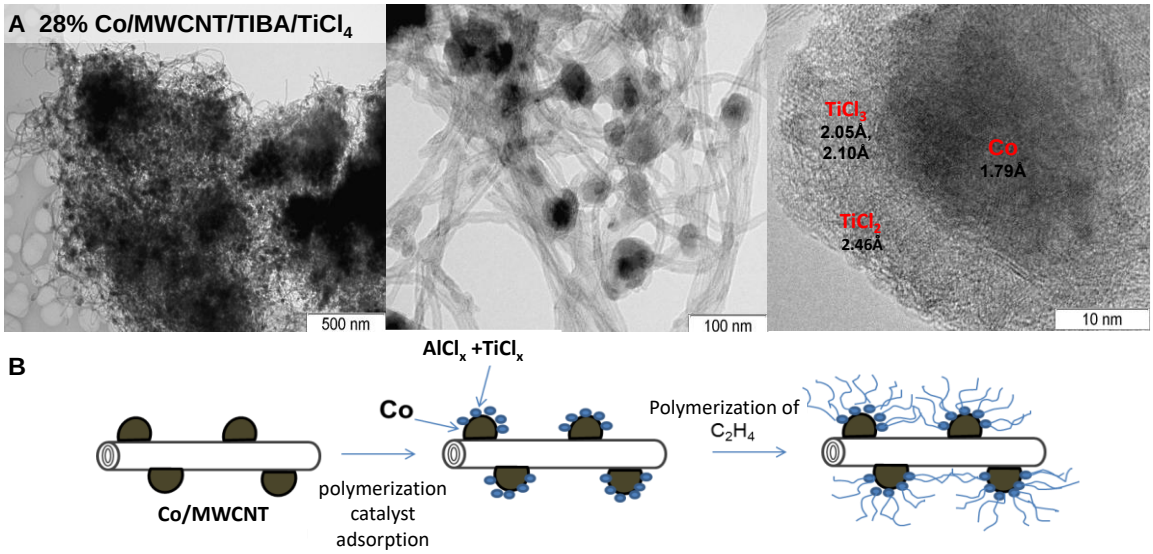

Fig. S4. A - TEM images of the polymerization catalytic system 28% Co/MWCNT/TIBA/$TiCl_4$; B - Schematic proposition of the localization of the Ti-containing polymerization catalyst on the surface of the Co/MWCNT hybrids.

X-ray diffraction of the Co/MWCNT-PE composites

The phase composition and crystal structure of Co/MWCNT-PE composites were investigated by powder XRD method using an ARL X'TRA diffractometer (Thermo Electron Corporation, Switzerland) equipped with the vertical theta geometry (Bragg-Brentano), Cu K-α radiation (λ = 0.15418 nm) and a Peltier cooled Si (Li) solid-state detector. The scanned 2θ range was from 18° to 70° in steps of 0.05° and a counting time of 3 s. Phase analysis was performed using the ICDD PDF-2 database.

The XRD patterns of Co/MWCNT-PE composites with different Co:MWCNT:PE component ratios are shown in Figure S5. They revealed that the Co/MWCNT-PE are composed of polyethylene, MWCNT and cobalt. No reflections of cobalt oxides could be detected, indicating that Co nanoparticles were preserved without oxidation due to the protective effect of polymer film. The XRD patterns were consistent with SEM and TEM images shown in Figure 4 (b-f). Two weak broad peaks of 2θ at 44.22°, and 51.52 ° were clearly observed for samples # 8 - 9 (with a Co loading of 2.8 and 3.8 wt. % in the samples), corresponding to the (111), and (200) plane of cobalt, respectively. It was difficult to estimate correctly the coherent scattering region (CSR) of Co nanoparticles in these samples due to the low Co loading. However, from the analysis of Co reflections, it can be unambiguously stated that the CSR was not less than 15 nm and not more than 50 nm. The reflections at 2θ ~ 25.91, 42.96 and 53.29 ° originated from the MWCNTs. However, only a weak reflection at 2θ ~ 25.9 ° was observed, since the other reflections were superposed with those of polyethylene.

The CSRs of PE, which corresponds to the mean size of the ordered (crystalline) domains of PE for MWCNT-PE and Co/MWCNT-PE composites were ~ 160 - 180 Å.

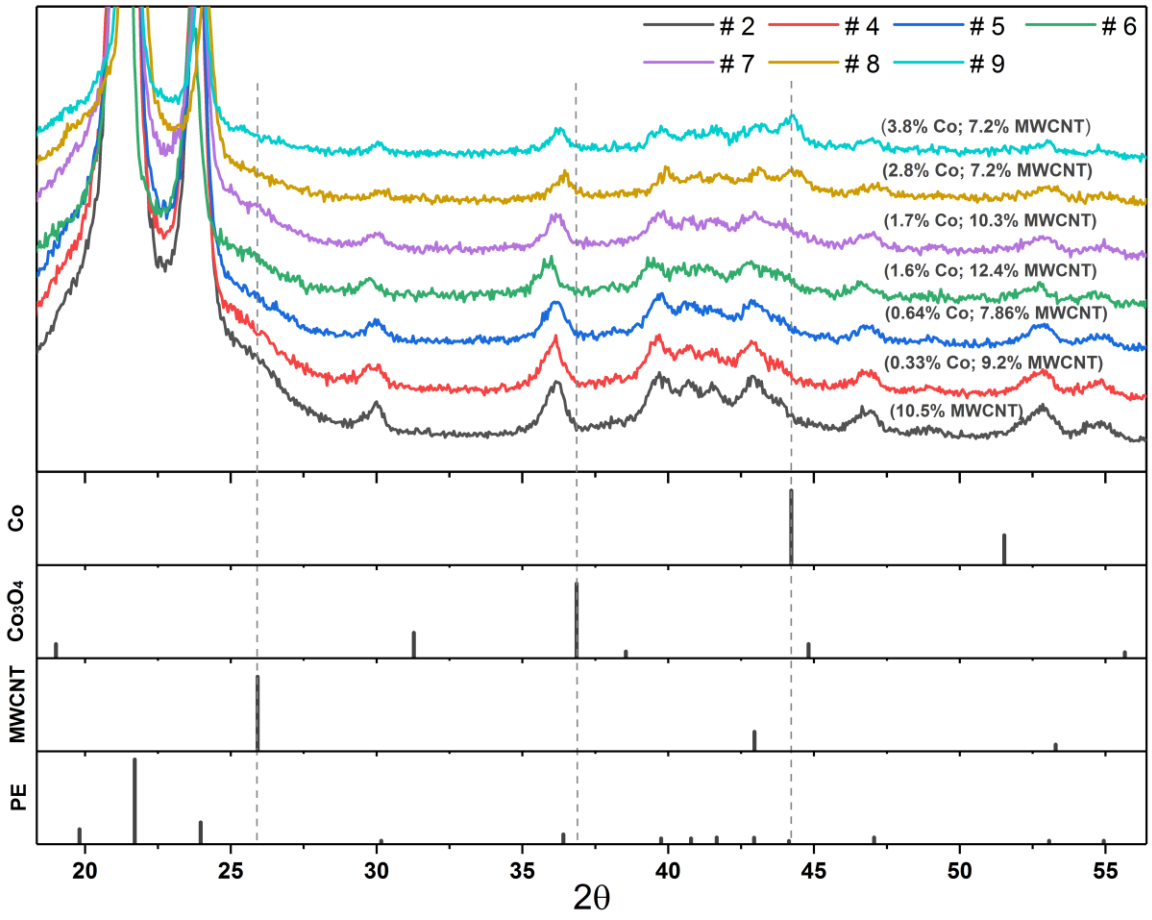

Fig. S5. XRD patterns of Co/MWCNT-PE composite samples with various component ratios (Co:MWCNT:PE).

Differential scanning calorimetry of the Co/MWCNT-PE composites.

The degree of crystallinity and melting point of the Co/MWCNT-PE composite materials depending on the filler composition (MWCNT or Co/MWCNT) were investigated by DSC using the DSC 204 F1 instrument (Netzsch, Germany) in accordance with ASTM D3418 - 15 procedure in an argon atmosphere (flow rate 30 mL min^{-1}) in closed 25-μL aluminium crucibles. The instrument was calibrated using reference samples based on indium (99.999%, Aldrich) and zinc (98+%, Aldrich) in accordance with the procedure [1]. The measurements were carried out in the melting–crystallization–melting mode in the temperature range of 25–180 °C at a rate of 10 deg min^{-1}. The melting point (T_m) and the enthalpy of melting were determined in the second melting cycle. The enthalpy of melting was calculated taking into account the content of MWCNT in the composite sample. The degree of crystallinity X was calculated using the Eq. 1:

$$X = (\Delta H_m/290) \times 100\% \qquad (1),$$

where ΔH_m is the enthalpy of melting of the sample (J g^{-1}), and 290 is the enthalpy of melting of ideal polyethylene with 100% crystallinity.

Table S1. DSC data for Co/MWCNT-PE composites.

# Samples	**Composition x wt.%(y wt.%Co/MWCNT)-PE**	**$T_{melting}$,°C***	**Crystallinity, X%**
Neat PE	Neat PE	138.0	58
2	10.5 MWCNT-PE	139.8	62
3	11.5 MWCNT-PE	138.3	57
4	9.5 (**3.5** Co/MWCNT)-PE	137.4	49
5	8.5 (**7.5** Co/MWCNT)-PE	138.1	50
6	14 (**11.5** Co/MWCNT)-PE	137.0	49
7	12 (**14.5** Co/MWCNT)-PE	136.9	50
8	10 (**28** Co/MWCNT)-PE	138.2	46
9	11 (**34** Co/MWCNT)-PE	139.5	47

* $T_{melting}$ corresponds to the maximum of the DSC crystallization curve of second melting recorded with a heating rate of 10°C/min.

According to the DSC data (Table S1), the introduction of different fillers such as MWCNTs and Co/MWCNT into the polyethylene matrix has no drastic influence on the melting point of the

polymer as all results lie in the range of 2–3 °C. However, the degree of crystallinity is more affected by Co/MWCNT filler composition (10–15 % change in comparison with neat polyethylene). On one hand, the melting point and degree of crystallinity remain high, and the shapes of the melting and crystallization peaks in the DSC curves are similar to those of the peaks of neat polyethylene (Fig. S5) indicating that the introduction of MWCNTs and Co/MWCNT into polyethylene does not lead to a significant disordering of its crystal structure. On the other hand, the existence of extensive fragments of crystalline polyethylene can be supposed.

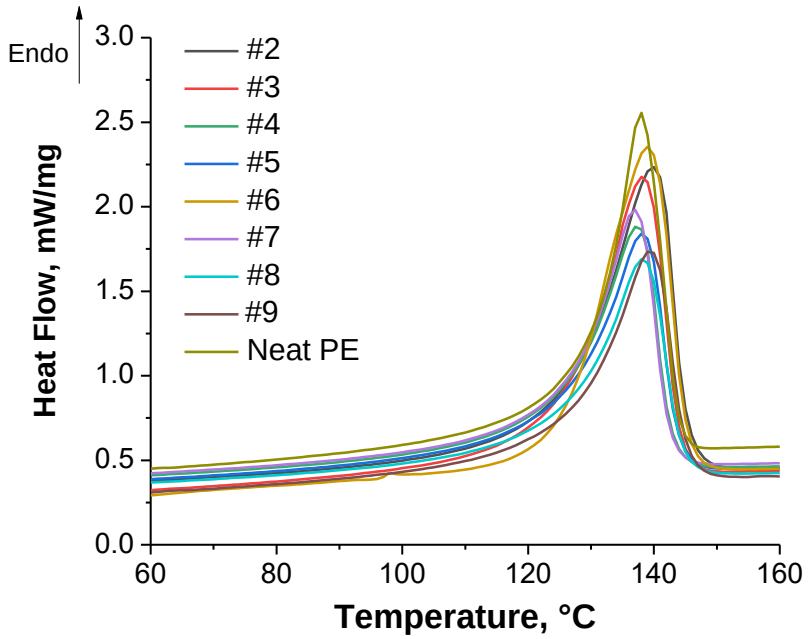

Fig. S6. Comparison of the second melting curves (DSC data) for the samples of neat PE, MWCNT-PE and Co/MWCNT-PE composites.

[1] V.A. Drebushchak, Calibration coefficient of a heat-flow DSC; Part II. Optimal calibration procedure, J. Therm. Anal. Calorim. 79(1) (2005) 213-218. 10.1007/s10973-004-0586-1

Table S2. The influence of the thickness of Co/MWCNT-PE composite material sample on the effective interaction region.

Sample #	Thickness, mm	Maximum RL, dB	Frequency at Maximum RL, GHz	Bandwidth range RL < 10 dB, GHz
4	4.0	-17.2	5.1	2.1
6	1.5	-11.7	12.6	3.3
6	4.0	-8.6	4.5	-
7	4.0	-55.0	5.2	1.8
7	1.5	-13.0	14.8	5.0
9	5.0	-27.8	17.2	1.3
9	4.0	-8.7	9.7	-

Table S3. Comparison and summary of EMI shielding properties of recently reported polymer composites containing various magnetic nanoparticles and nanostructured carbon materials.

Material	Total filler loading, wt.%	Magnetic components loading, wt.%	EMI shielding properties				Refs.
			Maximum RL, dB	Frequency at Maximum RL, GHz	Bandwidth range RL < 10 dB, GHz	Thickness, mm	
MWNTs/GO/Ni-PE-PEO	55	19.0	-70.0	17.1	-	5.0	[1]
PEDOT/RGO/Co_3O_4-paraffin	50	38.8	-51.1	10.7	9.4-12.5	2.0	[2]
FeCo@C@CNGs-paraffin	50	21.4	-67.8	15.8	13.0-18.0	1.75	[3]
Fe_3O_4/CNTs-paraffin	30	25.0	-58.6	15.3	14.0-18.0	1.5	[4]
Fe/Fe_3C@NCNTs - wax	30	15.3	-46.0	3.6	3.2−18.0	5.0	[5]
Fe_3O_4/CNTs-paraffin	30	22.5	-43.0	15.5	11.0-18.0	1.5	[6]
FeCo/MWCNT-PVDF	15	10.0	-55.0	9.6	-	5.0	[7]
Fe/CNT-epoxy	10	5.0	-31.7	13.2	11.8–14.7	1.0	[8]
Porous Co/C-paraffin	60	33.0	-35.3	5.8	5.0-7.0	4.0	[9]
α-Co/GN-paraffin	40	26.7	-47.5	11.9	10.0-14.0	2.0	[10]
Co/Gr flakes-polystyrene	40	10.0	-32.0	10.1	-	1.8	[11]
Co/C fibers-paraffin	33	12.0	-24.6	14.2	12.4−18	2.5	[12]
Co-filled MWCNTs-paraffin	20	8.0	-39.3	15.7	14.0-17.5	3.0	[13]
Co/CNTs-paraffin	20	8.6	-60.4	15.0	12.8-18	1.8	[14]
Magnetically aligned Co-C/MWCNTs-paraffin	15	5.6	-48.9	9.0	8.0-12.0	3.0	[15]
Co/MWCNT-PE	12	1.7	-55.0	5.2	4.3-6.1	4.0	This work
Co/MWCNT-PE	12	1.7	-13.0	14.8	12.8-17.8	1.5	This work

References

[1] P.K.S. Mural, S.P. Pawar, S. Jayanthi, G. Madras, A.K. Sood, S. Bose, Engineering Nanostructures by Decorating Magnetic Nanoparticles onto Graphene Oxide Sheets to Shield Electromagnetic Radiations, ACS Appl. Mater. Interfaces 7(30) (2015) 16266-16278. https://doi.org/10.1021/acsami.5b02703

[2] P.-B. Liu, Y. Huang, X. Sun, Excellent Electromagnetic Absorption Properties of Poly(3,4-ethylenedioxythiophene)-Reduced Graphene Oxide–Co_3O_4 Composites Prepared by a Hydrothermal Method, ACS Appl. Mater. Interfaces 5(23) (2013) 12355-12360. https://doi.org/10.1021/am404561c

[3] F. Wang, N. Wang, X. Han, D. Liu, Y. Wang, L. Cui, P. Xu, Y. Du, Core-shell FeCo@carbon nanoparticles encapsulated in polydopamine-derived carbon nanocages for efficient microwave absorption, Carbon 145 (2019) 701-711. https://doi.org/10.1016/j.carbon.2019.01.082

[4] X. Zeng, G. Jiang, L. Zhu, C. Wang, M. Chen, R. Yu, Fe_3O_4 Nanoflower-Carbon Nanotube Composites for Microwave Shielding, ACS Appl. Nano Mater. 2(9) (2019) 5475-5482. https://doi.org/10.1021/acsanm.9b01076

[5] Z. Xu, Y. Du, D. Liu, Y. Wang, W. Ma, Y. Wang, P. Xu, X. Han, Pea-like Fe/Fe_3C Nanoparticles Embedded in Nitrogen-Doped Carbon Nanotubes with Tunable Dielectric/Magnetic Loss and Efficient Electromagnetic Absorption, ACS Appl. Mater. Interfaces 11(4) (2019) 4268-4277. https://doi.org/10.1021/acsami.8b19201

[6] N. Li, G.-W. Huang, Y.-Q. Li, H.-M. Xiao, Q.-P. Feng, N. Hu, S.-Y. Fu, Enhanced Microwave Absorption Performance of Coated Carbon Nanotubes by Optimizing the Fe_3O_4 Nanocoating Structure, ACS Appl. Mater. Interfaces 9(3) (2017) 2973-2983. https://doi.org/10.1021/acsami.6b13142

[7] I. Arief, S. Biswas, S. Bose, Tuning the Shape Anisotropy and Electromagnetic Screening Ability of Ultrahigh Magnetic Polymer and Surfactant-Capped FeCo Nanorods and Nanocubes in Soft Conducting Composites, ACS Appl. Mater. Interfaces 8(39) (2016) 26285-26297. https://doi.org/10.1021/acsami.6b07464

[8] D.-L. Zhao, X. Li, Z.-M. Shen, Preparation and electromagnetic and microwave absorbing properties of Fe-filled carbon nanotubes, J. Alloys Compd. 471(1–2) (2009) 457-460. http://dx.doi.org/10.1016/j.jallcom.2008.03.127

[9] Y. Lü, Y. Wang, H. Li, Y. Lin, Z. Jiang, Z. Xie, Q. Kuang, L. Zheng, MOF-Derived Porous Co/C Nanocomposites with Excellent Electromagnetic Wave Absorption Properties, ACS Appl. Mater. Interfaces 7(24) (2015) 13604-13611. https://doi.org/10.1021/acsami.5b03177

[10] G. Pan, J. Zhu, S. Ma, G. Sun, X. Yang, Enhancing the Electromagnetic Performance of Co through the Phase-Controlled Synthesis of Hexagonal and Cubic Co Nanocrystals Grown on Graphene, ACS Appl. Mater. Interfaces 5(23) (2013) 12716-12724. https://doi.org/10.1021/am404117v

[11] A. Ansari, M.J. Akhtar, Co/graphite based light weight microwave absorber for electromagnetic shielding and stealth applications, Mater. Res. Express 4(1) (2017) 016304. https://doi.org/10.1088/2053-1591/aa570c

[12] W. Li, H. Qi, F. Guo, Y. Du, N. Song, Y. Liu, Y. Chen, Co nanoparticles supported on cotton-based carbon fibers: A novel broadband microwave absorbent, J. Alloys Compd. 772 (2019) 760-769. https://doi.org/10.1016/j.jallcom.2018.09.075

[13] H. Lin, H. Zhu, H. Guo, L. Yu, Microwave-absorbing properties of Co-filled carbon nanotubes, Mater. Res. Bull. 43(10) (2008) 2697-2702. http://dx.doi.org/10.1016/j.materresbull.2007.10.016

[14] Y. Yin, X. Liu, X. Wei, R. Yu, J. Shui, Porous CNTs/Co Composite Derived from Zeolitic Imidazolate Framework: A Lightweight, Ultrathin, and Highly Efficient Electromagnetic Wave Absorber, ACS Appl. Mater. Interfaces 8(50) (2016) 34686-34698. https://doi.org/10.1021/acsami.6b12178

[15] Y. Yin, X. Liu, X. Wei, Y. Li, X. Nie, R. Yu, J. Shui, Magnetically Aligned Co–C/MWCNTs Composite Derived from MWCNT-Interconnected Zeolitic Imidazolate Frameworks for a Lightweight and Highly Efficient Electromagnetic Wave Absorber, ACS Appl. Mater. Interfaces 9(36) (2017) 30850-30861. https://doi.org/10.1021/acsami.7b10067